Alpha-Particle Emission Energy Spectra From Materials Used for Solder Bumps

Michael S. Gordon, Kenneth P. Rodbell, David F. Heidel, Conal E. Murray, Henry H. K. Tang,
Brendan Dwyer-McNally, and William K. Warburton

Abstract—**The emitted alpha particle energy distribution from solder bumps can show substantial surface emission which has a large impact on the modeled SEU rate. State-of-the art alpha-particle detectors are required to measure the low emissivity and energy distribution.**

Index Terms—**Alpha particles, energy spectrum, ionization detectors, low-background, solder bumps.**

I. Introduction

THE contribution to Single-Event Upsets (SEU) due to alpha-particles in the packaging materials can be inferred experimentally by performing SEU tests underground where the flux of terrestrial neutrons is very low. Autran *et al.* have shown experimentally that although the SEU rate from alpha particles has decreased with scaling, their share of the total SEU rate is larger than that from terrestrial neutrons [1]. Recently, Wrobel, *et al.* have shown these same trends by Monte Carlo modeling [2]. Their alpha particle model assumed that the source of the alpha-particle emission was from U contamination in a wafer and that the influence of only 90 ppt of Uranium corresponds to an alpha-particle emissivity of ~ 0.4 $\alpha/\mathrm{khr} - \mathrm{cm}^2$ (the reported emissivity of a wafer). Other sources of alpha particles in integrated circuits could come from the Pb and/or Sn alloys in the solder bumps that are used to wire the circuits, underfill used to encapsulate the solder bumps, or impurities in the BEOL materials. Clearly the contribution to SEU from alpha particles continues to play an important role in the total SEU rates and the emissivity and energy distribution of the alpha particles needs to be determined quantitatively.

In this paper, we show the first direct measurement of ultra-low emissivity Sn-alloys which show predominantly surface emission. Based upon the energy of the emitted alpha particles, the source of the alpha particles at the surface is $^{210}\mathrm{Po}$. For these measurements, we used an ionization counter from XIA, that has low background and the ability to measure the energy of the alpha particles emitted from the sample [3].

II. Direct Measurement of Alpha Particle Activity

Typical solder bump dimensions and their center-to-center distance, or pitch, are 100 $\mu\mathrm{m}$ diameter and 200 $\mu\mathrm{m}$ separation, respectively. Direct measurement of the alpha particle emissivity of solder bumps is very difficult due to their small size, and sparse coverage on a wafer. Roberson developed correction factors, assuming only surface emission need be applied to the cross sectional area, for features with topology because simply using the cross sectional area of a feature that rises above a flat plane bump will underestimate its activity [4]. In the simplest example of a thin cylinder with one face, emission comes from the face only, and the emission rate is given by

$$\varepsilon = \sigma \bullet \pi \bullet r^2 \qquad (1)$$

where σ is the emissivity in units of $\alpha/\mathrm{khr} - \mathrm{cm}^2$, and r is the radius of the cylinder. The generalization to a right circular cylinder of height h is

$$\varepsilon = \sigma \bullet \left[\pi \bullet r^2 + \frac{1}{2}(2\pi \bullet r \bullet h)\right] \qquad (2)$$

where the second term is due to emission from the sides of the cylinder, and the factor of 1/2 comes about since the alpha particles from the sides could be emitted away from or toward the planar detector.

The emission from a hemisphere, which the bumps resemble, is given by [4]

$$\varepsilon = \sigma \bullet A \left[2\left(1 - \frac{1}{\pi}\right)\right] \qquad (3)$$

where $A = \pi r^2$. So, the effective area per hemisphere is 1.36 A. The total emission from an array of hemispherical solder bumps on a semiconductor wafer can be represented by

$$\varepsilon_{TOT} = \sigma \bullet \frac{A}{L^2} \left[2\left(1 - \frac{1}{\pi}\right)\right] C \qquad (4)$$

where L is the pitch and C is the wafer area. For a 200 $\mu\mathrm{m}$ pitch layout, this effective area increases the cross sectional area of the solder bumps from 19.6% to 26.7%. So the effective area of all of the solder bumps on a 300 mm diameter wafer is only about 188 cm^2. For a direct alpha-particle flux measurement of the solder bumps, as shown by Gordon *et al.*, it would take nearly 320 hr to make a measurement of an emissivity of $1\alpha/\mathrm{khr} - \mathrm{cm}^2$ using a detector with a background of 2 cts/hr at a 90% confidence level [3].
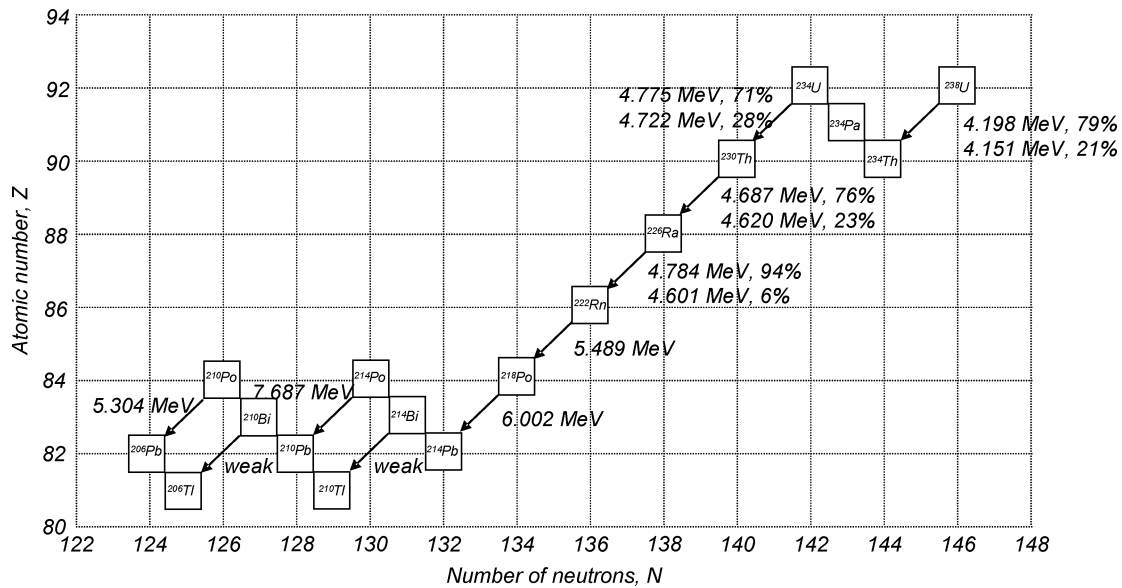
Fig. 1.   Chart showing the ^{238}U decay series. The decay of ^{210}Pb to ^{210}Po and the subsequent decay of a 5.3 MeV α-particle is shown at the end of the series [5].

Direct alpha-particle measurements from a Pb bulk-plated wafer or a sheet of Sn, using the same materials as those used for solder bumps therefore offer an attractive alternative to measurements of a wafer full of solder bumps since the plating covers the entire surface area of a wafer. For Sn-alloys, rolled samples can be fabricated in large, thin sheets. With either plated or large-area rolled samples, direct alpha-particle emission measurements can be accomplished more precisely in a shorter time than counting arrays of solder bumps.

III. ^{210}Po SEGREGATION, A HISTORY

For review, ^{210}Po is the daughter of ^{210}Pb, and also occurs near the end of the decay chain of ^{238}U, as shown in Fig. 1. ^{210}Pb decays by β emission to ^{210}Bi, which also decays by β emission to become ^{210}Po which emits a 5.3 MeV alpha particle. The full ^{238}U decay chain is shown in Fig. 1 where the principle alpha particle decays, decay probabilities, and alpha particle emission energies are highlighted.

After refinement of Pb or Sn, one expects that the majority of ^{238}U is removed, leaving only the decay of ^{210}Pb in leaded samples to be the source of the ^{210}Po. We expect the alpha particle activity to increase in time for a period of up to about 2.25 years before reaching secular equilibrium. The range of the 5.3 MeV alpha particles in lead is about 15 μm. For thick plated samples of Pb, containing ^{210}Pb, a triangular distribution of alpha particle emission as a function of detected energy is expected due to the attenuation of the number and energy of the alpha particles between the surface and $\sim$ 15 μm below the surface.

Fig. 2 shows the results of a simulation, using the Monte Carlo code SEMM2 [6], for emission of alpha particles from a thick sample of ^{210}Pb (solid line) and emission from the surface (dashed line). The solid curve shows the expected triangular distribution. The slight enhancement at the lowest energy bins is due to the increased number of paths high energy alpha particles can take which reduce their energy to the end of their range.

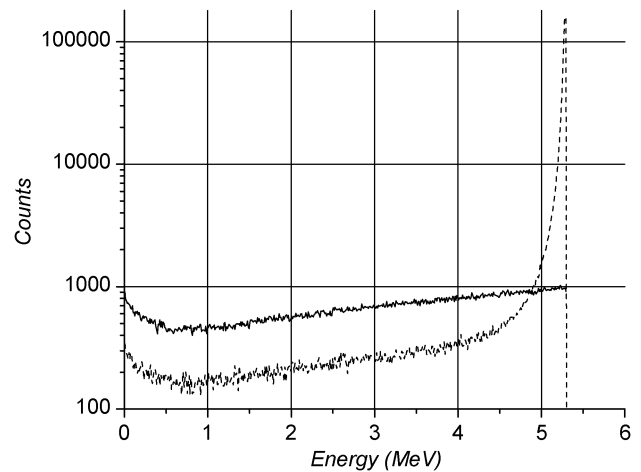As early as 1981, it was shown by Bouldin that the majority of alpha-particle emission from Pb/Sn solder was from ^{210}Po

Fig. 2.   Monte Carlo simulation of α-particle emission from a thick (solid line) source and surface emission (dashed line) from ^{210}Po.

occurring on the surface [7]. Additionally, Zabel, *et al.* in 1995 reported similar segregation of ^{210}Po to the surface in plated Pb/Sn films by examining the energy spectrum of emitted alpha particles $\frac{1}{2}$ year and $1\frac{1}{2}$ year after plating [8]. In both cases, the signature of the ^{210}Po segregation to the surface of the film was a pronounced peak in the alpha particle flux at 5.3 MeV.

The JEDEC specification, JESD89a, "Measurement and Reporting of Alpha Particle and Terrestrial Cosmic Ray-Induced Soft Errors in Semiconductor Devices" also makes mention of the "segregation of ^{210}Po to the surface of lead-based solders" [9]. No recommendations are made in this specification concerning the need to measure the energy spectrum from lead-based materials, or on the relative importance of the segregation on the counting rate of the bulk material.

Zastawny *et al.* presented a summary of experiments and a model to explain the observed migration of ^{210}Po to the surface of Pb samples [10]. The ^{210}Po atoms move to the surface by diffusion because the free energy of the atoms is lower at
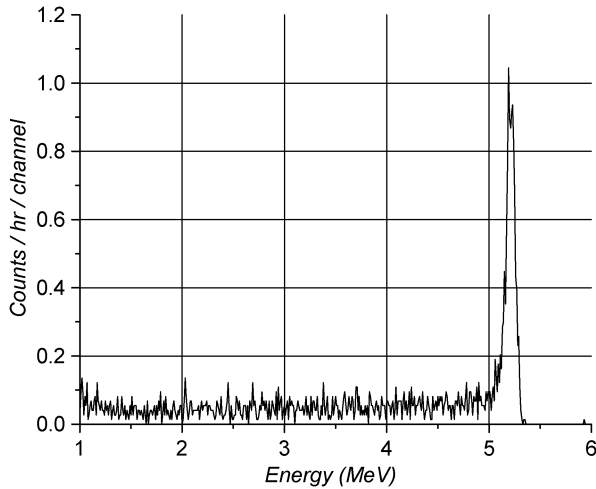
Fig. 3. Energy spectrum taken from a Sn sample which shows a significant amount of surface emission.

Fig. 4. Energy spectrum from a $\sim 90\ \alpha/\mathrm{min}\ ^{230}\mathrm{Th}$ source as measured in the XIA counter.

the surface than in the bulk lead. The authors observed an increase in alpha emission at higher temperature because of the increased diffusion coefficient. Interestingly, the surface segregation is eliminated for the bulk sample tested after two cycles of vacuum remelting.

Since there is a move in the semiconductor industry away from lead-based solder bumps, primarily from the health and safety concerns, to tin-based alloys solder bumps, it is important to determine whether or not a similar surface emission is observed in Sn, due to Pb, and/or U contamination.

IV. ENERGY SPECTRA FROM Sn-ALLOYS AND Pb PLATED WAFERS

Fig. 3 is an energy spectrum taken recently of a Sn sample showing significant surface emission. Integrating the alpha-particle spectrum, above 1 MeV, we determined the emissivity to be about 1500 $\alpha/\mathrm{khr} - \mathrm{cm}^2$ The peak at 5.3 MeV is from $^{210}\mathrm{Po}$ from either Pb or $^{238}\mathrm{U}$ contamination.

The integral of the emission spectrum over energy determines the emissivity of the sample. Samples with appreciable surface emission will have larger emissivity than comparable samples, of the same material, without surface emission due to the self-absorption of the alpha particle within the sample. For the model results shown in Fig. 2, for example, there were ~2.6X more alpha particles emitted from the surface (dashed line) compared to the bulk, 100 μm thick Pb sample (solid line), when identical number of alpha particles were emitted from the Monte Carlo generator.

The energy spectrum showing the $^{210}\mathrm{Po}$ emission at the surface of the plated materials from Fig. 3 was obtained using a silicon surface barrier detector, since the activity of the samples was large. Current commercially-available silicon detectors have backgrounds of about 50 $\alpha/\mathrm{khr} - \mathrm{cm}^2$ for detectors with area 4.5 cm^2 [11]. This background is clearly too large, and the area much too small, to make alpha particle measurements on ultra-low emissivity (e.g., $< 2\ \alpha/\mathrm{khr} - \mathrm{cm}^2$) films. Furthermore, to our knowledge, commercially-available silicon detectors are not available in sizes larger than 30 cm^2.
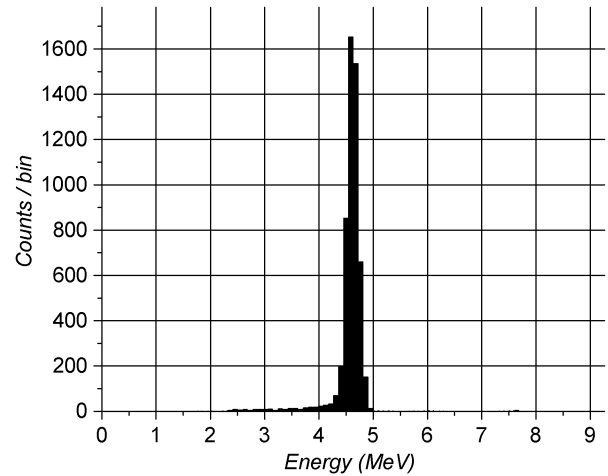
In 2009, Gordon *et al.* showed that the prototype XIA gas ionization counter could both measure very low emissivity samples, as well as produce an energy spectrum by making histograms of the anode pulse height distribution from a thick $^{210}\mathrm{Pb}$ radioactive source [3]. Commercially-available gas proportional counters do not provide energy information. These detectors achieve moderately-low background levels due both to a judicious choice of construction materials which provide passive shielding and by minimizing the volume of material in the active area. The result of this is that the range of alpha-particles is greater than the thickness of the counter gas used, precluding energy measurement. Because, in XIA's ionization counter, the anode-cathode distance is greater than the alpha-particle range to provide large signal amplitudes and to assist in active signal rejection, it also becomes possible to extract energy values as well [3]. The pulse height distribution in the ionization counter is proportional to the energy of the alpha particles.

Fig. 4 shows an energy spectrum from a $\sim 90\ \alpha/\mathrm{min}\ ^{230}\mathrm{Th}$ source placed on the center of the sample stage in the XIA counter. The anode pulse height was binned and converted to energy since the nominal energy from the $^{230}\mathrm{Th}$ alpha particles is known (α-energy: 4.62 MeV, 23.4%, 4.69 MeV, 76.3%) [5]. The energy resolution (FWHM) is about 6% so these peaks were not separately resolved. The measured efficiency (ratio of the measured number of counts to the NIST-traceable source activity) was 0.97 ± 0.02.

In this work, we used an XIA prototype ionization counter to measure the emissivity and energy distribution of alpha-particles of very low emissivity samples of Sn-alloy rolled sheets and Pb-plated wafers. The counter's low background allowed us to make accurate measurements quite rapidly.

Fig. 5 shows a histogram of the pulse height distribution, measured in the XIA counter for alpha particles from a thick, $\sim 1000\ \mathrm{cm}^2$, rolled sheet of an Sn alloy. The acquisition time was 67 hr. For reference, the measured emissivity of the sheet was $3.1 \pm 0.3\ \alpha/\mathrm{khr} - \mathrm{cm}^2$. The spectrum shows clear evidence of surface emission, with a substantial peak at $\mathrm{E} \sim 5.3\ \mathrm{MeV}$. The counter background was subtracted in a manner identical to that discussed in [3]. The energy spectra from two
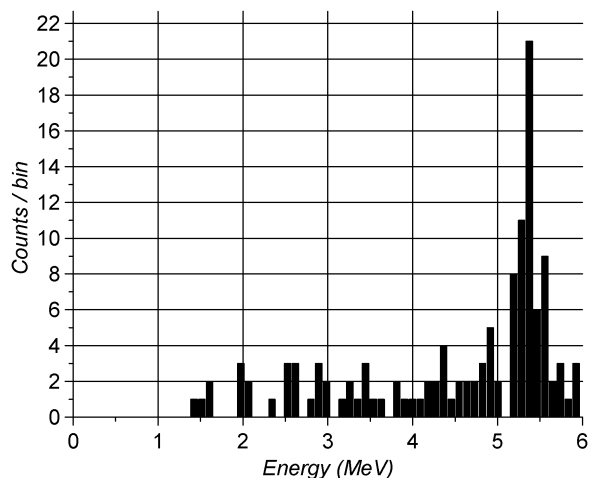
Fig. 5.   Pulse height spectrum from a rolled Sn-alloy, sample 506, 67 hr measurement time.
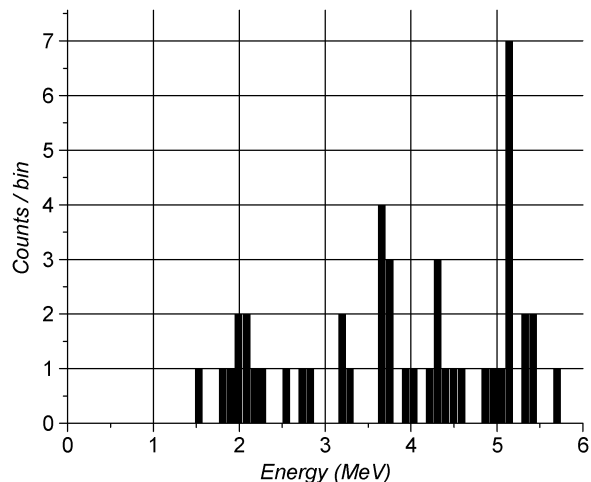

Fig. 8.   Pulse height spectrum from a rolled Sn-alloy, sample 803, 72 hr measurement time.
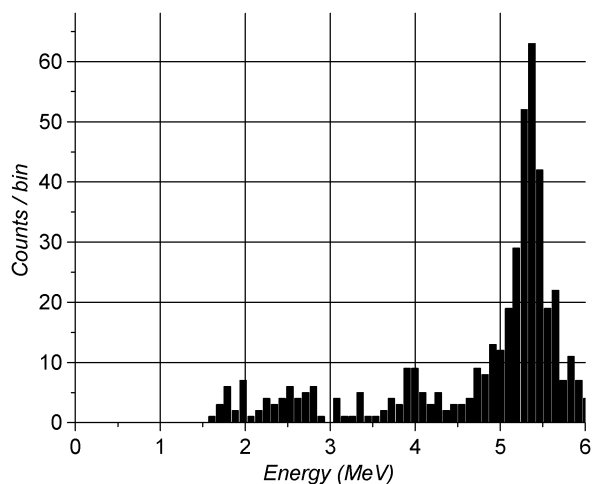

Fig. 6.   Pulse height spectrum from a rolled Sn-alloy, sample 505, 240 hr measurement time.
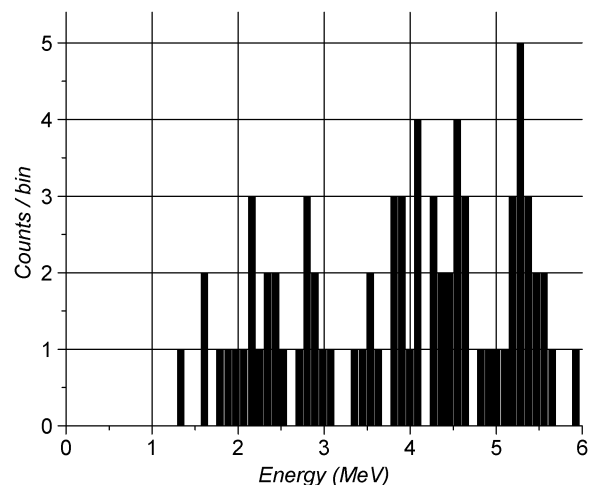

Fig. 9.   Pulse height spectrum from a rolled Sn-alloy sheet, sample 804, 85 hr measurement.

$0.3 \, \alpha/\mathrm{khr} - \mathrm{cm}^2$, respectively. These samples were measured for 240 hr and 48 hr, respectively. In each of these samples, about 60% of the total number alpha particles were emitted from the surface (near 5.3 MeV).

We also measured the alpha-particle emissivity and energy spectra of two rolled sheets of $\sim 1000 \, \mathrm{cm}^2$ Sn-alloy from another vendor. The alpha-particle emissivity for these samples and measurement times were: $1.2 \pm 0.2 \, \alpha/\mathrm{khr} - \mathrm{cm}^2$ (72 hr) and $1.6 \pm 0.2 \, \alpha/\mathrm{khr} - \mathrm{cm}^2$ (85 hr). The alpha-particle spectra for these samples are shown in Figs. 8 and 9. There is some evidence for surface emission in these samples; however, most of the alpha-particle emission occurs from within the volume, rather than the surface, especially for the sample shown in Fig. 9.

Finally, we measured the alpha-particle emissivity and energy spectra from three Pb-plated 200 mm wafers. The emissivity and measurement times of these wafers were: $25.1 \pm 1.9 \, \alpha/\mathrm{khr} - \mathrm{cm}^2$ (24 hr), $11.1 \pm 1.3 \, \alpha/\mathrm{khr} - \mathrm{cm}^2$ (24 hr), and $10.3 \pm 0.8 \, \alpha/\mathrm{khr} - \mathrm{cm}^2$ (69 hr), and the associated alpha-particle spectra for these samples are shown in Figs. 10–12, respectively. Clearly the peak, indicative of the alpha-particle emis-
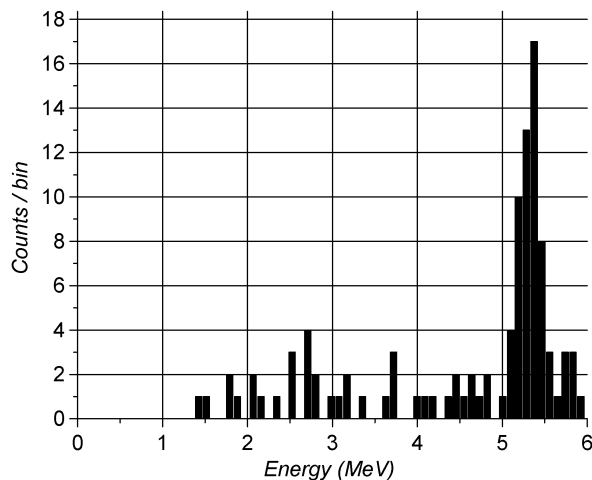

Fig. 7.   Pulse height spectrum from a rolled Sn-alloy, sample 504, 48 hr measurement time.

similar lots of rolled sheets of Sn-alloy from the same vendor as that shown in Fig. 5 are shown in Figs. 6 and 7, where the measured emissivities were $3.2 \pm 0.1 \, \alpha/\mathrm{khr} - \mathrm{cm}^2$ and $3.5 \pm$
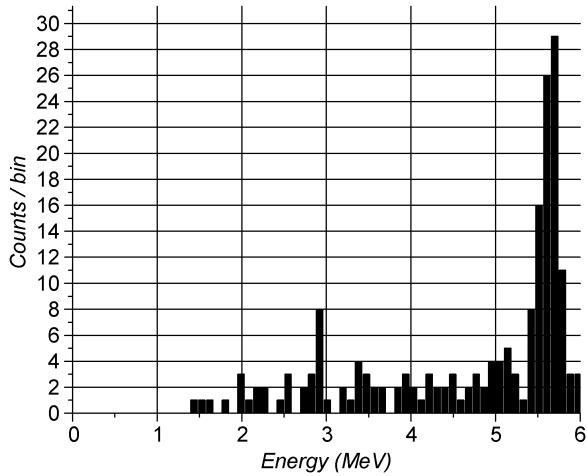
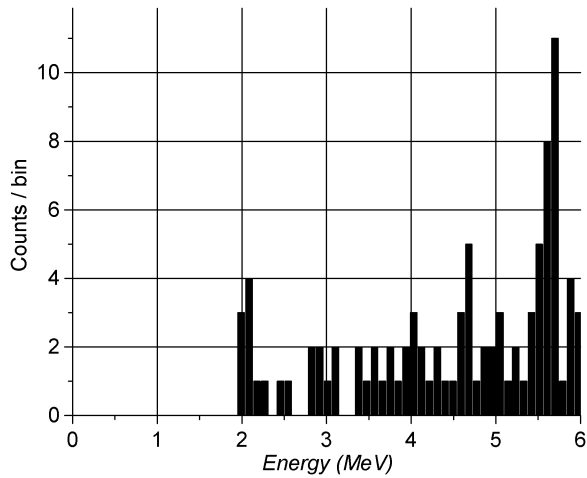Fig. 10. Pulse height spectrum from a plated Pb 200 mm wafer, #1, 24 hr.

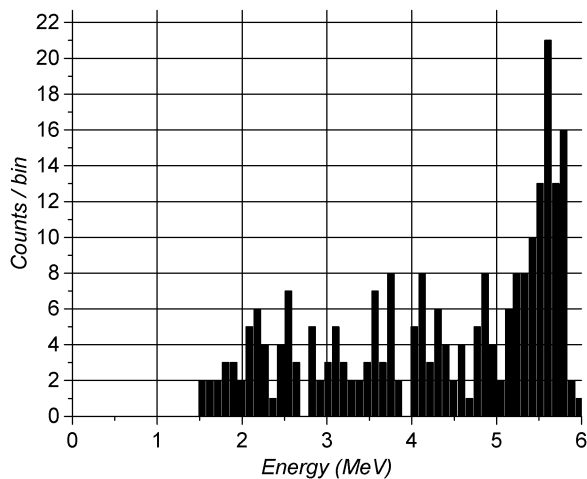Fig. 11. Pulse height spectrum from a plated Pb 200 mm wafer, #2, 24 hr.

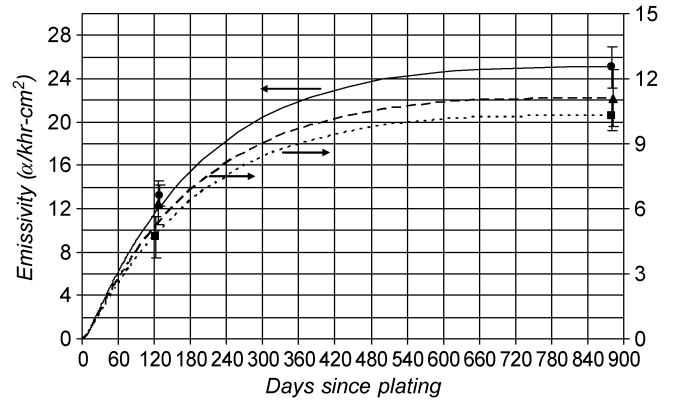Fig. 12. Pulse height spectrum from a plated Pb 200 mm wafer, #3, 69 hr.

Fig. 13. Emissivity of the three Pb-plated wafers as a function of days after plating. The units on the right-hand scale are the same as on the left-hand scale.
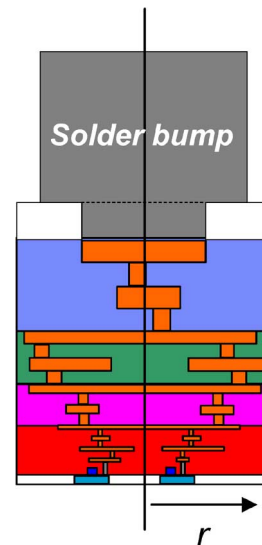

Fig. 14. Cross sectional schematic for BEOL geometry.

sion from ^{210}Po, is evident in each of the three samples. These Pb-plated wafers were plated in January 2008, and the alpha-particle emissivity had also been measured about 120 days after plating, T(120). In Fig. 13, we show the T(120) data and recent emissivity measurements for each wafer as a function of days after plating. Superimposed on the data are three curves showing the increase one would expect by secular equilibrium arguments, normalized to the recent alpha-particle emissivity. The left-hand scale (and solid line) goes with wafer 1 (circle), the right-hand scale goes with wafers 2 (dashed line, triangle) and 3 (dotted line-square). From the data in this figure, it is clear that the alpha-particle emission has increased as expected.

V. MODELING RESULTS

In 2009, Tang *et al.* showed modeling results of 45 nm SOI devices from the alpha particle emission from realistic solder bump geometries and circuit layouts [12]. The simulations reported in [12] assumed that the alpha-particle emitters were uniformly distributed within the solder bumps. The cross sectional schematic of the device modeled in [12] is shown below in Fig. 14.

Fig. 15 shows modeling results based on [12] for emission from a solder bump of 100 μm diameter and 60 μm height. The solder bump resides on a cylindrical pedestal which has a diameter of 50 um and height of 5 um. The emitted alphas go through a BEOL region which is approximately 10 μm thick. The relative alpha particle flux at the device level is plotted as a func-
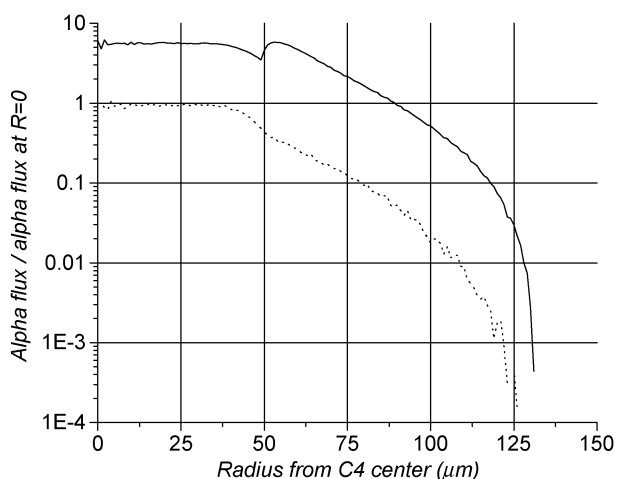
Fig. 15. Modeling results, based on [12], showing the difference in alpha particle flux between surface (solid line) and volume emission (dotted line).

tion of distance from the center of the solder bump. The relative flux is expressed as the flux at a given radius versus the flux at $r = 0$. Two simulations are compared using the same number of test particles. One calculation, shown by the solid line, is calculated with source points distributed uniformly on the solder bump (C4) surface, and the other, shown by the dotted line, is calculated with source points distributed uniformly throughout the volume of the solder bumps. The surface/volume emission ratio is ~6 under the solder bump $(r = 0)$ and continues to show a larger flux ratio beyond the edge of the solder bump. In realistic cases, because the flux from the solder bumps may be a combination of surface and volume emission, the effective ratio is expected to be less than 6. Nonetheless, the impact of surface emission, compared to volume emission, causes a larger alpha-particle flux below the solder bump which will further increase the alpha-particle component of SEU.

The impact on SEU rate of surface versus volume alpha-particle emission depends on several factors, including the alpha particle flux, the BEOL thickness, and the size and sensitivity of the memory or logic devices. Monte Carlo modeling of modern SRAMS has shown an increase in the SEU rate as large as 2–3X for surface emission versus volume emission.

VI. Summary

In this work, alpha particle emissivity measurements and the associated emission spectra were obtained from Sn-alloy sheets, and Pb-plated samples using a prototype ionization counter from XIA. This large-area, low-background counter, capable of measuring the energy of the alpha-particles, was necessary to make these measurements in a relatively-short period of time.

We believe this is the first published report showing extensive surface emission from ultra-low emissivity Sn-based samples. The level of surface emission in these Sn-based samples came as a surprise since the refinement process that produced the ultra-low levels of alpha-particle emission should have substantially reduced the U or Pb content in the tin. The substantial surface emission from the Pb-plated samples came as no surprise. In any event, the presence of surface emission changes the alpha-particle's energy distribution and, thus, the range of the alpha particles.

We conclude that any interpretation of alpha-particle emissivity data, therefore, must account for the presence or absence of surface emission for two reasons. First, surface emission causes an enhancement of the measured alpha-particle emission rates. Second, as in the modeling results for 45 nm SOI devices in [12], surface emission can significantly increase the SEU cross section compared to volume emission, which is usually assumed.

References

[1] J. L. Autran, P. Roche, S. Sauze, G. Gasiot, D. Munteanu, P. Loaiza, M. Zampaolo, and J. Borel, "Altitude and underground real-time SER characterization of CMOS 65 nm SRAM," in *Proc. 8th Eur. RADECS Workshop*, Jyvaskyla, Finland, Sep. 2008, pp. 319–324.

[2] F. Wrobel, F. Saigne, M. Gedion, J. Gasiot, and R. D. Schrimpf, "Radioactive nuclei induced soft errors at ground level," *IEEE Trans. Nucl. Sci.*, vol. 56, no. 6, pp. 3437–3441, Dec. 2009.

[3] M. S. Gordon, D. F. Heidel, K. P. Rodbell, B. Dwyer-McNally, and W. K. Warburton, "An evaluation of an ultralow background alpha particle detector," *IEEE Trans. Nucl. Sci.*, vol. 56, no. 6, pp. 3381–3386, Dec. 2009.

[4] M. W. Roberson, "Correction factors for area array alpha detectors," *J. Elect. Mat.*, vol. 29, no. 10, pp. 1270–1273, 2000.

[5] Chart of the nuclides. [Online]. Available: http://www.nndc.bnl.gov/chart/.

[6] H. H. K. Tang, "SEMM-2: A new generation of single-event-effect modeling tools," *IBM J. Res. Dev.*, vol. 52, no. 3, pp. 233–244, 2008.

[7] D. P. Bouldin, "The measurement of alpha particle emissions from semiconductor memory materials," *J. Elect. Mat.*, vol. 10, no. 4, pp. 747–795, 1981.

[8] T. Zabel, personal communication, 1995.

[9] [Online]. Available: http://www.jedec.org/standards-documents/results/jesd89a.

[10] A. Zastawny, J. Bialon, and T. Sosinki, "Migration of ^{210}Po in lead to the surface," *J. Radiat. Appl. Iso.*, vol. A38, no. 9, pp. 1147–1150, 1992.

[11] [Online]. Available: http://www.ortec-online.com/detectors/charged-particle/ultra.htm.

[12] H. H. K. Tang, C. E. Murray, G. Fiorenza, and K. P. Rodbell, "Modeling of alpha-induced single event upsets for 45 nm node SOI devices using realistic C4 and 3D circuit geometries," *IEEE Trans. Nucl. Sci.*, vol. 56, no. 6, pp. 3093–3097, Dec. 2009.